# Incorporation of Wind Effects Into Boussinesq Wave Models

Qin Chen[1]; James M. Kaihatu[2]; and Paul A. Hwang[3]

**Abstract:** Recent advances in the Boussinesq modeling of nearshore hydrodynamics offer a platform for the study of wind effects on wave transformation and breaking-generated nearshore circulation. The paper documents: (1) the new parameterization of the momentum flux transferred from the wind to surface gravity waves in the coastal region on the basis of the field observations; (2) the implementation of the parameterized wind stress into phase-resolving Boussinesq wave models; (3) the development of empirical breaking criteria with the wind effect based on the existing laboratory data; and (4) the tests of the extended Boussinesq model against field observations and empirical results with respect to wind drag coefficients over shoaling waves and wave growth on a shallow lake. Fairly good agreement between the model results and measurements is observed. The methodology for the parameterization of the wind stress as a function of wave steepness and wind speed as well as the extended Boussinesq model incorporating the wind forcing can be used as a tool to improve our understanding of wind effects on nearshore wave propagation and horizontal circulation.

**DOI:** 10.1061/(ASCE)0733-950X(2004)130:6(312)

**CE Database subject headings:** Air water interactions; Wind waves; Numerical models; Drag coefficient; Wind pressure; Hydrodynamics.

## Introduction

Coastal dynamics are intrinsically complex owing to the highly variable and nonlinear boundary conditions. Traditionally, we have focused on the influences of the seabed boundary on the nonlinear transformation of coastal waves, such as wave shoaling and refraction caused by bathymetric variations as well as depth-limited wave breaking on the beach. The effects of the wind forcing imposed on the ocean surface have also received much attention in connection with the study of wave generation in the deep ocean. In contrast, the wind effects on wave transformation and breaking in the nearshore ocean, extending from the surf zone to the water depth of about 10 m, have drawn much less attention in the literature.

Experienced surfers know that an offshore wind blowing from land to sea is usually associated with favorable surfing conditions, specifically plunging breakers. Galloway et al. (1989) conducted field measurements and revealed that offshore winds increase the number of plunging waves, and onshore winds increase the number of spilling waves. Douglass (1990), and King and Baker (1996), in a series of laboratory experiments, have also demonstrated the importance of wind speed and direction with regard to wave breaking, similar to the findings from Galloway et al.'s (1989) field observations. Unfortunately, quantification of wind effects on wave breaking is currently unavailable. The mechanism of wind effects on wave transformation and breaking in the shallow water is still unclear. Consequently, the wind effects on the generation of breaking-driven currents and resulting sediment transport in the littoral region are virtually unknown.

Recent advances in Boussinesq modeling of nearshore hydrodynamics have offered a platform for the study of wind effects on wave-induced horizontal circulation. Reviews on the recent development and applications of Boussinesq wave models were given by Madsen and Schaffer (1999) and Kirby (2003). Today, time-domain Boussinesq models are not only able to simulate nearshore propagation of nonlinear waves, but are also capable of predicting breaking-induced cross-shore and alongshore currents with remarkable accuracy, as demonstrated by Chen et al. (1999, 2003), among others. A natural step forward is to parameterize the wind stress and incorporate it into the Boussinesq model aimed at quantifying the wind influence on coastal waves and breaking-induced nearshore circulation.

The paper is organized as follows. First, we present the new parameterization of the momentum flux transferred from the wind to surface gravity waves in the coastal region on the basis of the field observations of enhanced wind stress by shoaling waves. Next, we show how to implement the parameterized wind stress into a phase-resolving Boussinesq wave model. After that, the wind effect on wave breaking is incorporated into the Boussinesq model based on the existing laboratory experiments. Then tests of the forced Boussinesq model against field observations and empirical results are given. As an application, we simulate longshore currents with and without the wind effect to examine the response of a current to the change in wave breaking caused by a wind. Finally, we summarize the findings.

[1]Assistant Professor, Dept. of Civil Engineering, Univ. of South Alabama, Mobile, AL 36688. E-mail: qchen@jaguar1.usouthal.edu

[2]Oceanographer, Ocean Dynamics and Prediction Branch, Oceanography Division, Code 7322, Naval Research Laboratory, Stennis Space Center, MS 39529-5004.

[3]Supervisory Oceanographer, Oceanography Division, Naval Research Laboratory, Stennis Space Center, MS 39529-5004.

Note. Discussion open until April 1, 2005. Separate discussions must be submitted for individual papers. To extend the closing date by one month, a written request must be filed with the ASCE Managing Editor. The manuscript for this paper was submitted for review and possible publication on July 21, 2003; approved on July 20, 2004. This paper is part of the ***Journal of Waterway, Port, Coastal, and Ocean Engineering***, Vol. 130, No. 6, November 1, 2004. ©ASCE, ISSN 0733-950X/2004/6-312–321/$18.00.

## Parameterization of Air–Sea Momentum Flux

### *Field Evidence of Enhanced Air–Sea Momentum Flux by Shoaling Waves*

Field observations of air–sea momentum flux over shoaling waves were conducted by Anctil and Donelan (1996) who measured wind velocity components (i.e., downwind velocity $u$ and vertical velocity $w$) and surface waves simultaneously along a cross-shore transect from 12.5 to 3 m water depth in Lake Ontario. They estimated the air–sea momentum flux from the covariance of measured velocities at the anemometer height using the eddy correlation method and inferred the drag coefficient $C_d$. The wind stress on the sea surface may be expressed as

$$\tau = -\rho_a \overline{uw} \tag{1}$$

where $\rho_a$=air density and the over bar denotes time average. The drag coefficient is then estimated by

$$C_d = \frac{\tau}{\rho_a U_{10}^2} = -\frac{\overline{uw}}{U_{10}^2} \tag{2}$$

in which $U_{10}$=wind speed at 10 m above the sea level under the neutrally stable boundary layer condition.

Fig. 1 shows the inferred drag coefficient, wave age, and wave steepness along the cross-shore transect. It is seen that the drag coefficient increases as the water depth decreases before wave breaking. Inside the surf zone, wave breaking reduces the wave steepness and consequently reduces the drag coefficient. The ratio of the wind speed at 10 m above the sea level to the peak wave celerity is the inverse of the wave age. Obviously waves become younger as the water depth decreases because of the reduction of the wavelength, or wave celerity.

The air–sea momentum flux can be parameterized using the aerodynamic surface roughness length. On the basis of the field data, Anctil and Donelan (1996) suggested that the surface roughness length $z_0$ was expressed as a function of wave age

$$\frac{z_0}{H_{\mathrm{mo}}} = A\left(\frac{U_{10}}{C_p}\right)^B \tag{3}$$

in which $H_{\mathrm{mo}}$=zero moment wave height; and $C_p$=peak wave celerity. The empirical coefficients $A=9.25\times10^{-5}$ and $B=3.22$ were obtained by a regression analysis of the field data. More recently, Taylor and Yelland (2001) proposed an alternative to Eq. (3). They suggested that the surface roughness length was expressed as a function of wave steepness

$$\frac{z_0}{H_{\mathrm{mo}}} = A_1\left(\frac{H_{\mathrm{mo}}}{L_p}\right)^{B_1} \tag{4}$$

where $L_p$=peak wavelength; and $A_1$=1,200 and $B_1$=4.5 are regression coefficients. Taylor and Yelland (2001) indicated that Eq. (4) gave a better representation of a variety of existing data sets.

The wind speed profile in the atmospheric boundary layer near the sea surface may be approximated as (e.g., Hsu 1988)

$$\frac{U_z}{u_*} = \frac{1}{\kappa}\left[\ln\left(\frac{z}{z_0}\right) - \Psi_m\left(\frac{z}{L}\right)\right] \tag{5}$$

where $z$=anemometer height; $U_z$=wind speed measured at $z$; $u_*=(\tau/\rho_a)^{1/2}$=friction velocity; and $\kappa=0.4$=von Karman constant. The stability length $L$ depends on the difference between the air temperature $\theta_a$ and the sea surface temperature $\theta_s$. The empirical function $\Psi_m$ is a linear function of $z/L$ in the stable case ($\theta_a>\theta_s$ or $L>0$) and a nonlinear function of $z/L$ in the unstable case ($\theta_a<\theta_s$ or $L<0$) (see, e.g., Hsu 1988). At 10 m above the sea level under the neutrally stable boundary layer condition, we have $\Psi_m=0$, as $\theta_a=\theta_s$ or $L\to\infty$. Thus Eq. (5) becomes

$$\frac{U_{10}}{u_*} = \frac{1}{\kappa}\ln\left(\frac{10}{z_0}\right) \tag{6}$$

Upon the use of Eq. (2) and the definition of friction velocity, an arrangement of Eq. (6) leads to the relationship between the drag coefficient and the surface roughness length $z_0$, as used by Anctil and Donelan (1996)

$$C_d = \left(\frac{\kappa}{\ln(10/z_0)}\right)^2 \tag{7}$$

Eqs. (3), (4), and (7) will serve as a reference for the wind stress implemented into the Boussinesq wave model, as discussed in the following sections.

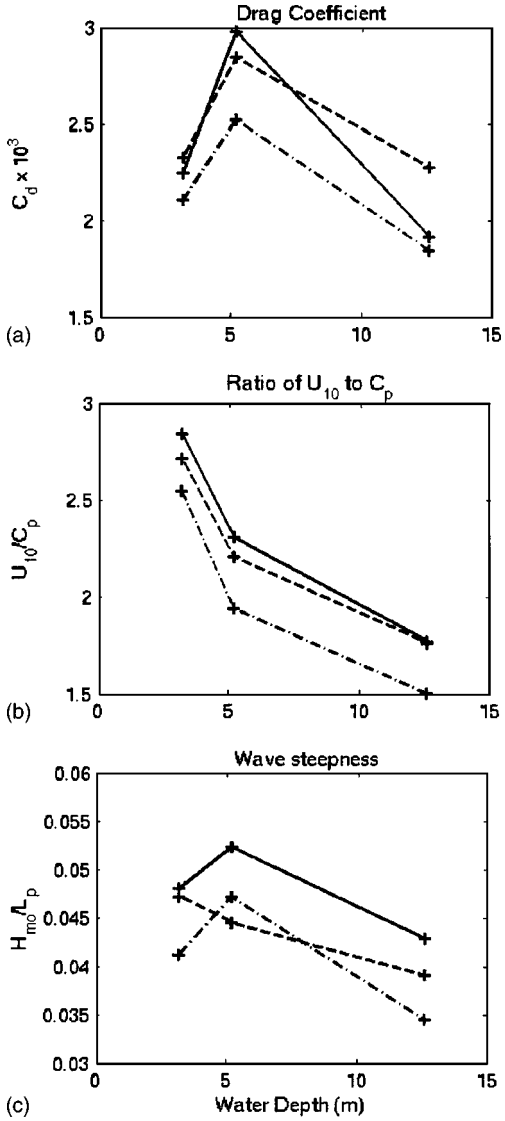


**Fig. 1.** Drag coefficient (a) inverse of wave age, (b) wave steepness, and (c) as function of water depth: (solid lines) $\overline{U_{10}}$ =15.1 m/s, (dashed line) $\overline{U_{10}}$=14.2 m/s, and (dashed-dotted lines) $\overline{U_{10}}$=13.6 m/s; data source: Anctil and Donelan (1996)

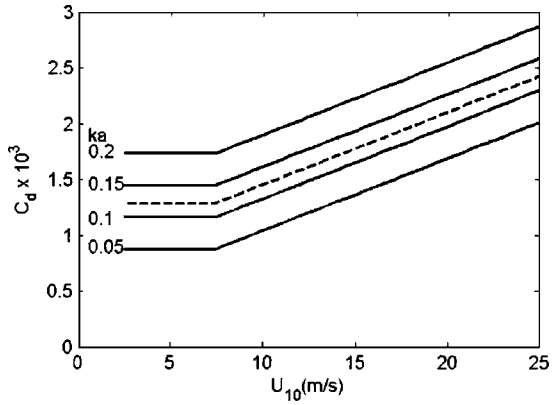


**Fig. 2.** Drag coefficient as function of wind speed and wave steepness (solid lines); dashed line is Wu's (1980) drag coefficient

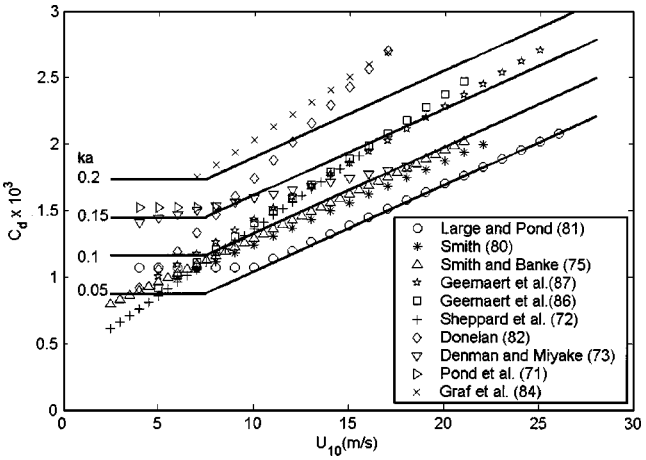


**Fig. 3.** Comparison of Eq. (8) with drag coefficient formulas complied by Geernaert (1990)

### *Parameterization of Momentum Flux*

The momentum flux transferred from winds to surface waves in the time-domain Boussinesq wave model may be parameterized as the wind stress, $\boldsymbol{\tau}=\rho_a C_d \mathbf{U}|\mathbf{U}|$, where $\mathbf{U}$=wind velocity vector at a reference elevation, and $C_d$=corresponding drag coefficient. Suggested by the field evidence, the wind drag coefficient in the coastal zone must be a function of not only the wind speed, but also the geometry of the surface gravity waves that are often skewed and asymmetrical owing to the seabed boundary. We propose a new formula of drag coefficient as follows:

$$C_d 10^3 = (a_1 + a_2|\eta_x|) + bU_{10} \tag{8}$$

where $a_1$, $a_2$, and $b$=empirical coefficients, and $\eta_x$ =instantaneous surface slope computed in the Boussinesq model. Phase average of the drag coefficient allows for a comparison of the new formula with conventional drag coefficient formulas, such as the equation proposed by Wu (1980).

Fig. 2 illustrates the phase-averaged drag coefficient as a function of wind speed and wave steepness, $ka$ ($k$=wave number and $a$=wave amplitude). We choose $a_1=0.2$, $a_2=18$, and $b=0.065$. The wave steepness ranges from 0.05 to 0.2 with an increment of 0.05. It is seen that the new drag coefficient increases with both wind speed and wave steepness. Following Wu (1980), the third term in Eq. (8) is set to be 0.4875 for wind speed less than 7.5 m/s. The dashed line in Fig. 2 depicts the drag coefficient given by Wu

$$C_d 10^3 = 0.8 + 0.065U_{10} \tag{9}$$

which is only a function of wind speed. The curves of the new drag coefficient are parallel to Wu's curve and the offset depends on the wave steepness.

In addition to Wu (1980)'s equation, a large number of empirical formulas for the drag coefficient have been proposed in the literature (see e.g., Geernaert 1990). Each formula represents the best fit to a specific dataset. Fig. 3 shows a comparison of the new drag coefficient and the existing formulations. It is seen that the scattering of the drag coefficient as a function of the wind speed may be explained by the effect of the sea state, or the wave steepness. Statistically, Eq. (8) agrees fairly well with all the data, which is not achieved by any single existing formula of drag coefficient.

One of the crucial differences in airflow over steep surface waves in comparison to the flow over a flat surface is the presence of a form drag due to the separation of airflow. Laboratory measurements of the tangential and normal stresses on the air–water interface (Banner and Peirson 1998) suggest that the form drag accounts for the major proportion of the wind stress once the waves have developed beyond their early growth stage. The most interesting scenario of wind effects on coastal waves is the strong wind condition. We hypothesize that the separation of airflow occurs on the lee side of the wave crest in the shallow water and, consequently, the form drag is a dominant contributor to the momentum flux between the atmosphere and the nearshore wave field. The hypothesis is in line with the sheltering theory proposed by Jeffreys (1925) as a mechanism of wave generation.

The time-domain Boussinesq model resolves the individual wave motion and predicts reasonably well the geometry of the surface waves distorted by the seabed, such as the skewness and asymmetry of the waves in the shallow water (e.g., Chen et al. 2000 and Shi et al. 2003). The wind stress implemented into the Boussinesq model should vary over a wavelength, with a larger drag coefficient on the wave crest than that in the trough to take the form drag into account. In fact, only the heterogeneous distribution of the wind stress over a wavelength allows for changes of wave height by a wind in a phase-resolving wave model. Assuming that the form drag is dominant over the skin friction, we apply the wind stress on the wave crest only, neglecting the effect of the shear stress on the wave trough in the Boussinesq model. It is worth mentioning that other forms of parameterization may be possible.

The temporal and spatial variation of drag coefficient is one of the important features of the wind stress on the nearshore waves simulated by the phase-resolving Boussinesq model. With the instantaneous wave celerity and wave slope obtained from the computed surface elevation at each grid and every time step, the wind stress is calculated as a function of the wind velocity relative to the wave celerity as well as the wave slope in the following form:

$$\tau = C_d \rho_a |U_{10} - C|(U_{10} - C) \tag{10}$$

where $C$=instantaneous wave celerity estimated in the Boussinesq model. Eq. (10) is similar to the wind stress formulation followed by Schwab et al. (1984) in a wave prediction model on the basis of a phase-averaged momentum balance equation rather than an energy balance equation.

## Extended Boussinesq Wave Model

The formulation of the wind stress is implemented into the Boussinesq wave model developed by Wei et al. (1995), Kennedy et al. (2000), and Chen et al. (2000, 2003). In order to take into account the short waves generated by local winds, we also extend the dispersion accuracy of the one-dimensional version of the model to $kh=6$ ($h$=still water depth) by introducing the additional terms from Madsen and Schaffer's (1998) equations into the model. A new set of coefficients for better shoaling properties of the equations (Madsen personal communication 2002 and Kennedy et al. 2002) is also implemented into the model. In one horizontal dimension, the extended Boussinesq equations read

$$\eta_t + M_x = 0 \tag{11}$$

where

$$M = (h+\eta)\left[u_\alpha + \left(\frac{z_\alpha^2}{2} - \frac{1}{6}(h^2 - h\eta + \eta^2)\right)u_{\alpha xx} + \left(z_\alpha + \frac{1}{2}(h-\eta)\right) \times (hu_\alpha)_{xx}\right] + (\beta_2 - \beta_1)h^2((h+\eta)u_\alpha)_{xx} - \beta_2(h^2((h+\eta)u_\alpha)_x)_x + (\beta_2 - \beta_1)h^2\eta_{xt} - \beta_2(h^2\eta_t)_x \tag{12}$$

and

$$u_{\alpha t} + u_\alpha u_{\alpha x} + g\eta_x + \Lambda_0 + \Lambda_1 + \Lambda_2 + \Lambda_3 - R_b - R_s + R_f - R_w = 0 \tag{13}$$

where

$$\Lambda_0 = \left(\frac{z_\alpha^2}{2} + (\alpha_2 - \alpha_1)h^2\right)u_{\alpha xxt} + (z_\alpha - \alpha_2 h)(hu_{\alpha t})_{xx} + (\alpha_2 - \alpha_1)h^2\eta_{xxx} - \alpha_2 h(h\eta_x)_{xx} \tag{14}$$

$$\Lambda_1 = \left[z_\alpha u_\alpha (hu_\alpha)_{xx} + \tfrac{1}{2}z_\alpha^2 u_\alpha u_{\alpha xx} - \eta(hu_{\alpha t})_x + \tfrac{1}{2}((hu_\alpha)_x)^2\right]_x + \tfrac{1}{2}(\alpha_2 - \alpha_1)h^2(u_\alpha^2)_{xxx} - \tfrac{1}{2}\alpha_2 h(h(u_\alpha^2)_x)_{xx} \tag{15}$$

$$\Lambda_2 = \left[\eta u_{\alpha x}(hu_\alpha)_x - \eta u_\alpha (hu_\alpha)_{xx} - \tfrac{1}{2}\eta^2 u_{\alpha xt}\right]_x \tag{16}$$

$$\Lambda_3 = \left[\tfrac{1}{2}\eta^2(u_{\alpha x})^2 - \tfrac{1}{2}\eta^2 u_\alpha u_{\alpha xx}\right]_x \tag{17}$$

In the equations, $\eta$ free surface elevation relative to the still water level; $u_\alpha$=velocity at the reference elevation $z_\alpha(=-0.54122h)$ in the water column; and the subscripts $t$ and $x$ denote time and spatial differentiations, respectively. The dispersion enhancement coefficients with improved shoaling properties are $(\beta_1, \beta_2) = (0.03917, 0.315236)$ and $(\alpha_1, \alpha_2) = (0.01052, 0.124537)$. The additional terms, $R_b$, $R_s$, $R_f$, and $R_w$ represent the effects of wave breaking, subgrid lateral turbulent mixing, seabed shear stress, and wind stress, respectively. Detailed descriptions of the first three terms can be found in Chen et al. (1999). Upon the use of Eq. (10), we obtain

$$R_w = \frac{\rho_a}{\rho(h+\eta)}C_d|U_{10} - C|(U_{10} - C) \tag{18}$$

where $\rho$=water density.

The internal wavemaker for the generation of random waves at the offshore boundary is extended to accommodate the enhancement of dispersion properties in the Boussinesq equations. In comparison to Wei et al.'s (1995) model, the additional terms in Eq. (12) require the solution of a tridiagonal system for the continuity equation.

Other extensions of the model include the modification of the breaking criteria in the model to account for the energy dissipation owing to whitecaps. The original breaking criteria in Kennedy et al. (2000) were designed for depth-limited wave breaking. The basic idea is to replace the still water depth $h$ by $C^2/g$ where $g$ is the gravitational acceleration. This leads to the modified criteria for the onset ($\eta_t^{(I)}$) and cessation ($\eta_t^{(F)}$) of wave breaking as follows:

$$\eta_t^{(I)} = \gamma_1 C \tag{19}$$

$$\eta_t^{(F)} = \gamma_2 C \tag{20}$$

in which $\gamma_{|1}=0.35-0.65$ and $\gamma_{|2}=0.15$. We choose the lower limit of $\gamma_{|1}$ in the presence of a wind that is in the direction of the wave train. Other terms with $h$ in the breaking scheme of Kennedy et al. (2000) are also modified in a similar fashion.

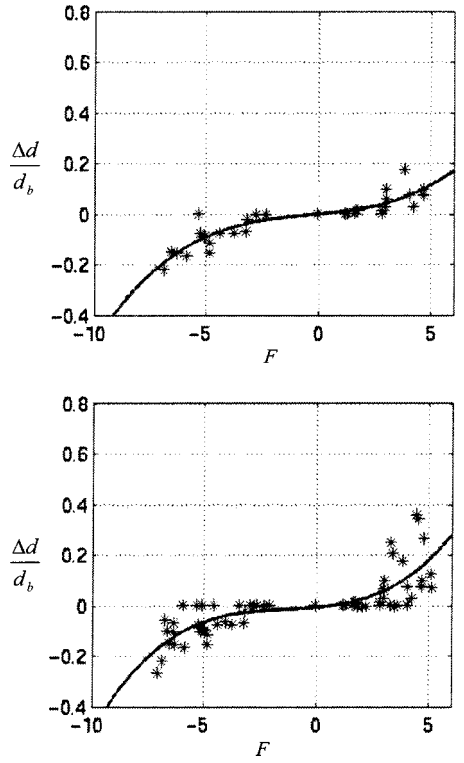


**Fig. 4.** Wind effects on breaking locations from King and Baker (1996): (top) spilling breakers; (bottom) spilling and plunging breakers

## Wind Effect on Wave Breaking

### *Laboratory Data*

King and Baker (1996) presented data sets of laboratory experiments on the wind effect on depth-limited wave breaking. Their work is an extension of the physical experiment conducted by Douglass (1990) with the improvement in the modeling of the air boundary layer. The model scales are 1:50 and 1:100 for the water wave and the airflow, respectively. Fig. 4 shows the measured

breaking locations as a function of wind speed in King and Baker's (1996) experiment. The horizontal axis is the Froude number defined as

$$\mathsf{F} = \frac{U}{\sqrt{gH_p}} \tag{21}$$

where $U$=wind speed at a reference elevation and $H_p$=wave height near the wave maker. The vertical axis is the difference in the breaker depths with and without a wind ($\Delta d$) normalized by the breaker depth in the presence of a wind ($d_b$). A positive $\mathsf{F}$ corresponds to a wind blowing onshore and a negative $\mathsf{F}$ corresponds to a wind blowing offshore. It is seen that an onshore wind tends to cause an early occurrence of breaking and vice versa for an offshore wind. In other words, an onshore wind causes waves to break further offshore in the deeper water while an offshore wind causes waves to break further onshore in the shallower water in comparison to the case without a wind, if the change in the water level due to the wind is small. It appears from the laboratory experiments that spilling and plunging breakers respond to the wind effect somewhat differently.

Both experiments conducted by Douglass (1990) and King and Baker (1996) were focused on the wind effect on wave breaking in the shallow water. They found that the breaker height was hardly affected by the wind speed and direction. Because of the change in the breaker depth in the presence of a wind, the ratio of wave height to water depth at the breaking location appears to be a function of wind speed and direction, in addition to the beach slope and offshore wave steepness.

### *Empirical Breaking Criteria*

The mechanism of the wind influence on depth-limited wave breaking was hypothesized as a microbreaking process (Douglass 1990) or as a vortical effect resulting from the wind velocity shear (King and Baker 1996). This small scale breaking mechanism is not taken into account by any conventional macrobreaking criteria. Therefore, new empirical breaking criteria as a function of the wind speed are developed for the extended Boussinesq model on the basis of the laboratory data. A cubic curve fitting of the spilling and plunging data in Fig. 4 yields

$$f_r = \frac{\Delta d}{d_b} = (0.067F^3 + 0.26F^2 + 0.79F)0.01 \tag{22}$$

As $\Delta d = d_b - d_{b0}$, where $d_{b0}$=breaker depth without a wind, we have

$$d_b = \frac{d_{bo}}{1 - f_r} \tag{23}$$

Combining the shoaling and wind effects, we obtain the empirical breaking criterion

$$\eta_t^{(I)} = \lambda C \tag{24}$$

where

$$\lambda = 0.65(1 - f_r)^{0.75} \tag{25}$$

Fig. 5 illustrates the effect of an onshore wind on wave breaking over a barred beach. The solid lines sketch the wave profile with rollers near the bar crest and close to the shoreline. In the case of an onshore wind, the Froude number is positive and so is $f_r$. Thus Eq. (25) yields a coefficient smaller than 0.65 that is the default coefficient calibrated by Kennedy et al. (2000) in the absence of a wind. With a smaller criterion for the onset of breaking, the waves will break in the deeper water as illustrated by the dashed lines in Fig. 5, and vice versa for the case of an offshore wind.

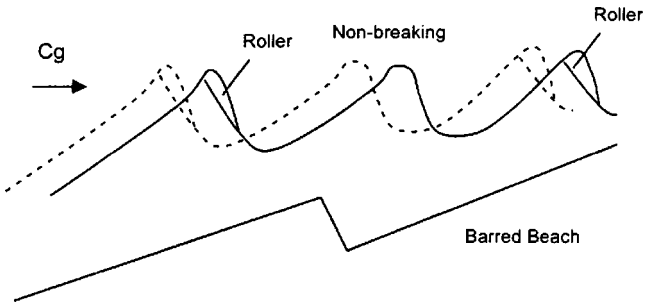


**Fig. 5.** Schematic of wave breaking on barred beach with (dashed lines) and without (solid lines) an onshore wind

Notice that the above equations are derived from the laboratory data for the depth-limited wave breaking. It may not be extended to the steepness-limited breaking. Furthermore, caution needs to be taken when using the breaking criteria under conditions different from the laboratory because of the scaling problems. Nevertheless, we demonstrate a procedure that can be used to develop breaking criteria with the wind effect if simultaneous field measurements of breaking location and wind speed are available.

## Model Tests

### *Drag Coefficient over Shoaling Waves*

Anctil and Donelan's (1996) field experiment on air–sea momentum flux over shoaling waves provides us with an excellent data set to test the wind stress we introduce to the Boussinesq model. However, a direct simulation of the data set is difficult because the extended model with better dispersion properties is limited to one horizontal dimension and $kh < 6$. Thus we opt to compare the drag coefficient derived from the Boussinesq model results to the drag coefficients computed from the formulas developed by Anctil and Donelan (1996) and Taylor and Yelland (2001).

Fig. 6 shows the bathymetry and the cross-shore variations of the wave age and wave steepness in this test case. The horizontal axis is the distance from the wave maker in the Boussinesq model. We construct the bathymetry using the measured water depth at four instrumentation locations. The offshore wave conditions are taken from an average of three measurements, which gives the zero moment wave height $H_{\mathrm{mo}}$=0.9 m and the peak wave period $T_p$=5.3 s at the offshore water depth of 8.4 m. Because no measured wave spectra are available, we use a relatively broad Texel–Marsden–Arslo (TMA) spectrum (Bouws et al. 1985) with the shape parameter $\gamma$=2.0. The wind speed is $U_{10}$=7.0 m/s and remains constant in the computation domain. The peak wave celerity and peak wavelength are calculated from the linear wave theory, and the wave height is given by the Boussinesq model. Waves become shorter due to the shoaling effect. It is seen that both the inverse of the wave age and wave steepness increase rapidly in the wave depth shallower than 3 m near the shoreline.

Inserting the wave age and wave steepness into Eqs. (3) and (4), respectively, we obtain the surface roughness length. Direct use of Eq. (7) yields the drag coefficient that is a function of the

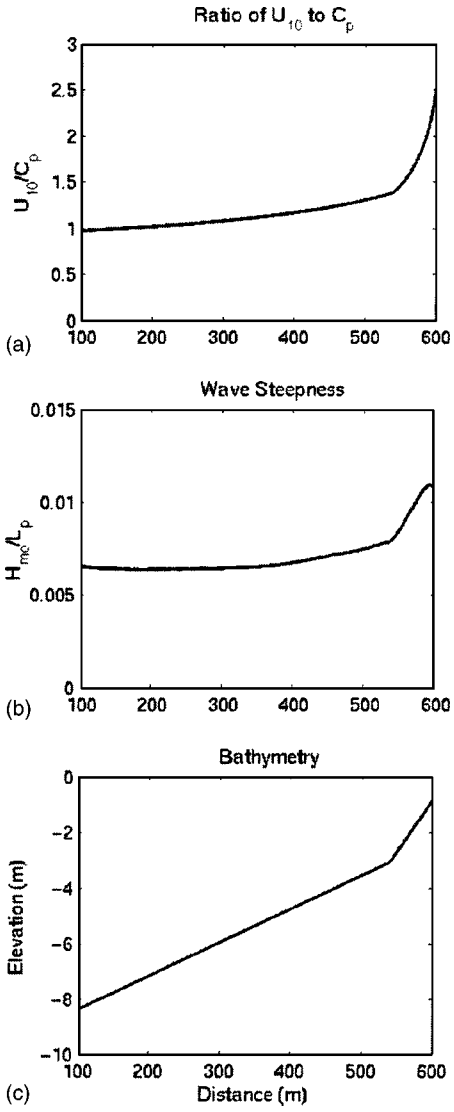


**Fig. 6.** Cross-shore variations of (a) inverse of wave age, (b) wave steepness, and (c) bathymetry in case of $U_{10}=7.0$ m/s

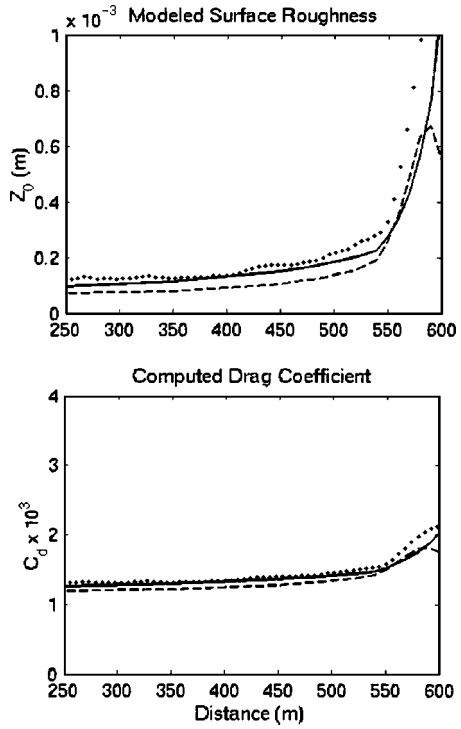


**Fig. 7.** Cross-shore variations of surface roughness (top) and drag coefficient (bottom) in case of $U_{10}=7.0$ m/s: (solid lines) Anctil and Donelan (1996), (dashed lines) Taylor and Yelland (2001), and (dotted line) Boussinesq model

surface roughness. Conversely, solving Eq. (7) with a phase-averaged drag coefficient from the Boussinesq model leads to the corresponding surface roughness length. Fig. 7 shows the cross-shore variations of the surface roughness length predicted by the both formulas and the comparison of the drag coefficients derived from the Boussinesq model and Eq. (7). It is seen that both Anctil and Donelan's (1996) and Taylor and Yelland's (2001) formulas predict very similar surface roughness of the wave field from the Boussinesq model except for the area very close to the shoreline where wave breaking reduces the wave steepness. We notice that the phase-averaged drag coefficient given by the Boussinesq model agrees very well with the drag coefficients using the estimated surface roughness length. Similar agreement is observed between the surface roughness lengths inferred from the phase-averaged drag coefficient and the wave fields.

The second test case has a wind speed of $U_{10}=14.1$ m/s, a zero moment wave height $H_{\mathrm{mo}}=2.13$ m, and a peak wave period $T_p=6.8$ s at the offshore water depth of 8.6 m. Similar to the first test case, a TMA shallow water wave spectrum with the shape parameter $\gamma=2.0$ is employed as the offshore boundary condition. Fig. 8 shows the bathymetry and the cross-shore variations of the wave age and wave steepness in this test case. The storm surge caused by the strong wind increases the offshore water depth by 20 cm in comparison to the previous case. Because of the larger offshore wave height, wave breaking reduces the wave steepness near the shoreline, as shown in Fig. 8(b). By contrast, the wave age decreases monotonically from the deep water to the shoreline. It is anticipated that both Anctil and Donelan's (1996) and Taylor and Yelland's (2001) formulas predict different surface roughness length in the surf zone.

Fig. 9 depicts the cross-shore variations of the surface roughness length predicted by both Anctil and Donelan's (1996) and Taylor and Yelland's (2001) formulas as well as the phase-averaged drag coefficient, and the comparison of the drag coefficients derived from the Boussinesq model and Eq. (7). Similar to Fig. 7, both formulas predict very similar surface roughness length of the wave field given by the Boussinesq model except for the shallow water where wave breaking reduces the wave steepness. Fair agreement is observed between the phase-averaged drag coefficient given by the Boussinesq model and the drag coefficients obtained from the estimated surface roughness length and Eq. (7), except for the region close to the shoreline. The roughness length inferred from the phase-averaged drag coefficient predicted by the Boussinesq model, however, amplifies the differences.

In general, the model results in both test cases agree fairly well with the drag coefficients inferred from field measurements outside the surf zone. This indicates that the parameterization of the drag coefficient incorporated into the Boussinesq model is a reasonably good representation of the air–sea momentum flux over the shoaling waves.

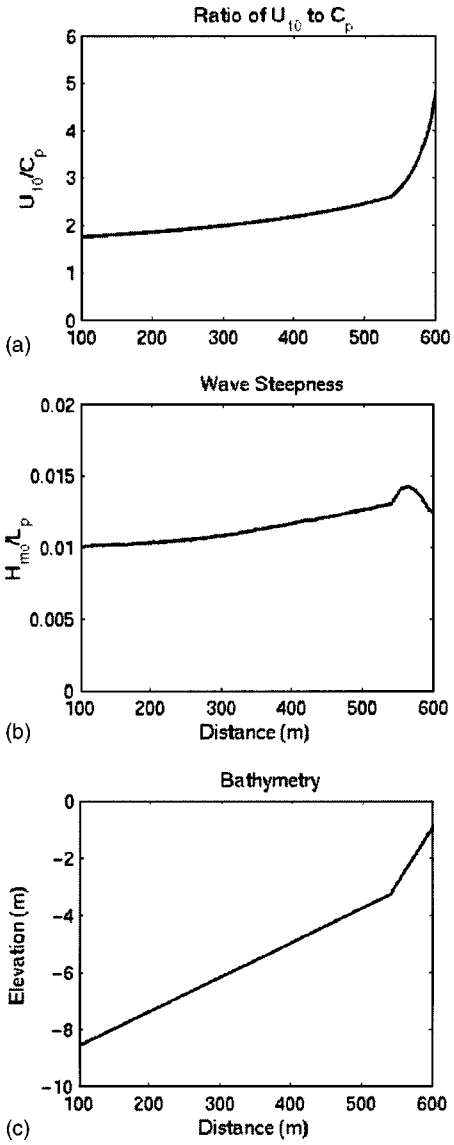


**Fig. 8.** Cross-shore variations of (a) inverse of wave age, (b) wave steepness, and (c) bathymetry in case of $U_{10}=14.07$ m/s.

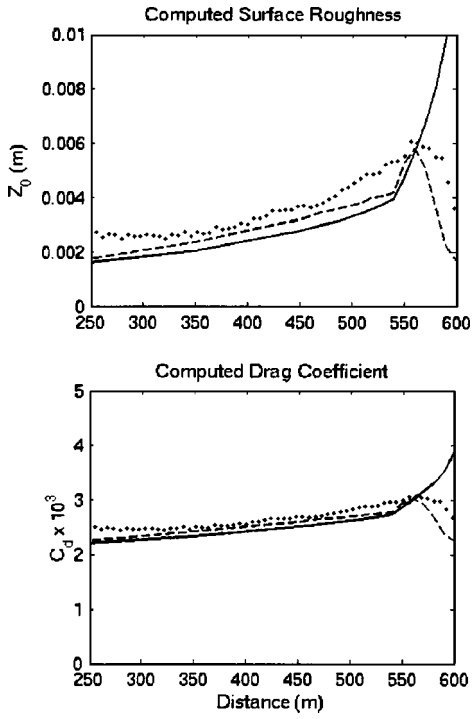


**Fig. 9.** Cross-shore variations of surface roughness (top) and drag coefficient (bottom) in case of $U_{10}=14.1$ m/s: (solid lines) Anctil and Donelan (1996), (dashed lines) Taylor and Yelland (2001), and (dotted line) Boussinesq model

### *Wave Growth on Shallow Lake*

The test cases in the preceding section concentrate on the surface roughness length and drag coefficient associated with shoaling waves over a distance of about 500 m. Can the wind stress implemented into the Boussinesq model simulate the growth of wind waves over a longer fetch? We shall address such a question using the data set of wave growth in Lake George, Australia collected by Young and Verhagen (1996).

Lake George is a shallow lake with a typical water depth of 2 m. It is about 20 km long and 10 km wide. A series of eight observation stations were deployed along the north–south fetch to measure the wind waves. The wave data collected by Young and Verhagen (1996) under a nearly ideal condition have served as a test bed for a number of phase-averaged wave models, such as simulating waves nearshore (Booij et al. 1999). We choose two data sets corresponding to a medium wind speed of $U_{10}=10.8$ m/s and a large wind speed of $U_{10}=15.2$ m/s to test the wind stress formulation incorporated into the Boussinesq model. Owing to the dispersion limit of the Boussinesq model ($kh<6$), only the observations at the last four stations (5–8) are utilized. The fetch between Stations 5 and 8 is about 4.25 km. The up-wave boundary condition is taken from the observation at Station 5 where the zero-moment wave height is $H_{\mathrm{mo}}=0.367$ m and the peak wave period is $T_p=2.34$ s in the case of a moderate wind ($U_{10}=10.8$ m/s), and $H_{\mathrm{mo}}=0.473$ m and $T_p=2.4$ s in the case of a strong wind ($U_{10}=15.2$ m/s). We use TMA shallow water wave spectra with the shape parameter $\gamma=3.3$ at the up-wave boundary as the input to the Boussinesq model. A bottom friction coefficient of $f=0.0005$ is used in the quadratic law of the bottom shear stress (Chen et al. 1999).

Fig. 10 shows comparisons of the computed and measured significant wave heights and wave periods as well as the computed and inferred drag coefficients under the moderate wind condition. It is seen that the wave heights predicted by the Boussinesq model are in fairly good agreement with the field measurements. The computed peak wave periods, however, do not agree with the observations. The wind stress incorporated into the Boussinesq model simply does not lead to the increase of the wave period along the fetch. The downshift of the peak frequency is absent in the modeled wave energy spectrum. This is attributed to the inability of the Boussinesq model to take quadruplet interactions into account and to describe the full process of wave growth. Interestingly, the phase-averaged drag coefficient calculated from the Boussinesq model is in good agreement with the coefficient estimated using the modeled wave characteristics and Anctil and Donelan's (1996) formula. The drag coefficients given by Taylor and Yelland's (2001) formula (triangles), however, are smaller than either Boussinesq or Anctil and Donelan's result (solid line and squares).

Similar comparisons are made for the case of large wind speed as shown in Fig. 11. Again, the Boussinesq model predicts the growth of wave height fairly well in comparison to the field mea-

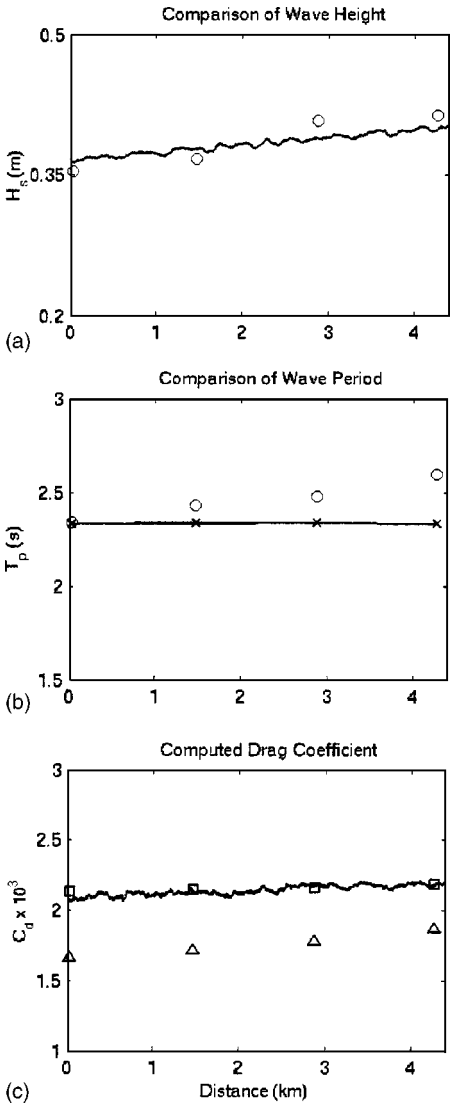


**Fig. 10.** Comparisons of computed and measured significant wave heights (a) computed and measured peak wave periods, (b) computed and inferred drag coefficients, and (c) in case of $U_{10}$=10.8 m/s: (solid lines) Boussinesq model results, (circles) Young and Verhagen's (1996) observations, (squares) Anctil and Donelan (1996), and (triangles) Taylor and Yelland (2001)

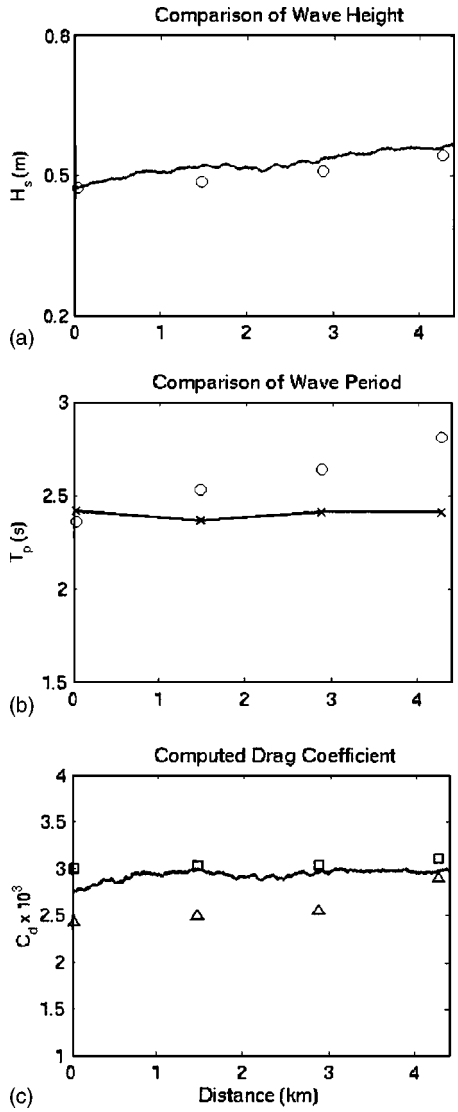


**Fig. 11.** Comparisons of computed and measured significant wave heights (a) computed and measured peak wave periods, (b) as well as computed and inferred drag coefficients, and (c) in case of $U_{10}$=15.2 m/s: (solid lines) Boussinesq model results, (circles) Young and Verhagen's (1996) observations, (squares) Anctil and Donelan (1996), and (triangles) Taylor and Yelland (2001)

surements but considerably underpredicts the increase of wave period. The agreement among the drag coefficients is also very similar to the case with a moderate wind. The phase-averaged drag coefficient obtained from the Boussinesq model agrees better with Anctil and Donelan's result than does Taylor and Yelland's formula, as shown in Fig. 11(c). Notice that all the drag coefficients are computed using the wave field given by the one-dimensional Boussinesq model, which is not able to predict the downshift of the peak frequency. It should be pointed out that the Boussinesq model with the wind forcing is not able to simulate wave growth from a calm sea or small ripples that eventually grow to larger waves. Nevertheless, the prediction of wave height growth under both moderate and strong wind conditions by the Boussinesq model confirms that the new formulation of wind stress is a reasonable representation of the momentum flux transferred from a wind to surface waves in nearshore regions in a phase-resolving model.

## Wind Effect on Longshore Currents

Recently, Chen et al. (2003) and Chen (2004) introduced a procedure to transform Boussinesq-type equations derived from the assumption of potential flow into a wave-current model by consistently recovering the vertical component of vorticity associated with wave-driven currents. Longshore currents generated by the breaking of obliquely incident waves on a natural beach were successfully simulated by Chen et al. (2003) using an enhanced Boussinesq model. However, wind forcing was not included in their simulations. Field observations have shown that winds can contribute considerably to the measured longshore currents (e.g., Hubertz 1986). For a wind blowing obliquely from sea to land, the alongshore component of the wind stress will either enhance or reduce the magnitude of the wave-induced longshore current, depending on the wind and wave directions. On the other hand, the cross-shore component of the wind stress will cause setup of

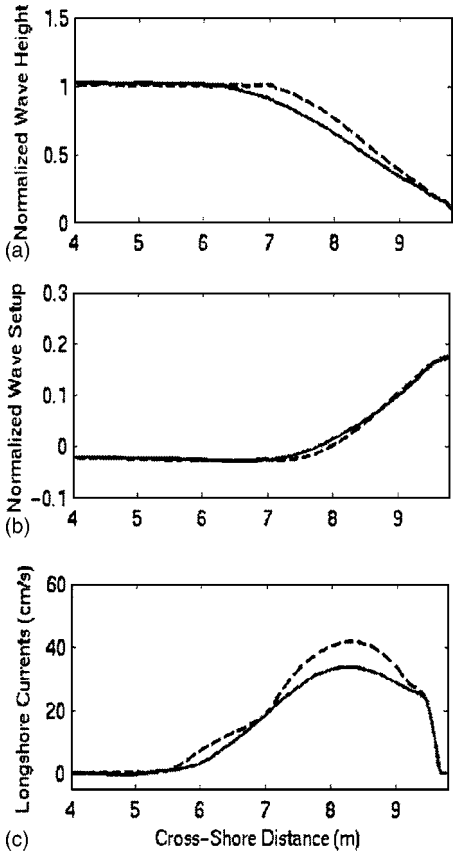


**Fig. 12.** Compariaon of model results with and without a wind: (a) wave height, (b) wave setup, and (c) longshore currents: (solid lines) onshore wind, (dashed lines) no wind

the mean sea level, or storm surge. In principle, a Boussinesq model covering a large domain can predict both the wind-generated current and setup, but a nondispersive shallow-water model is computationally more suitable for such simulations than Boussinesq models.

Besides those well known wind effects on the nearshore water, Douglass (1990) suggested that the change in the breaking location by a wind could impact the wave-generated longshore current and sediment transport. We shall examine such an impact using the extended, two-dimensional Boussinesq wave model incorporating the wind effects. Because the breaking criteria were developed using laboratory data, we restrict our numerical experiment to a planar beach at the laboratory scale. The slope of the planar beach is 1:20, which starts from an offshore water depth of 35 cm. The obliquely incident, regular wave train has an amplitude of 3.9 cm, a period of 1.02 s, and an angle of 15.4° in the offshore depth. The setup of the numerical wave basin is similar to the well known Visser's (1991) laboratory experiments on longshore currents without a wind.

Fig. 12 compares the computed wave heights, mean water levels, and longshore currents with and without a wind. With the new breaking criteria, the extended Boussinesq model predicts an earlier occurrence of wave breaking under an onshore wind condition in comparison to the case without a wind. The magnitude of the Froude number for the wind reaches eight. It is seen that although the cross-shore variation of wave setup is slightly affected by the change in the breaking location, the maximum wave setup is barely influenced by the wind because of the very short fetch in this case. A larger wind-induced setup is anticipated for a larger model domain.

One of the interesting results of this idealized numerical experiment is the prediction of a weaker longshore current under an onshore wind in comparison to the case without a wind. The change in the surf zone width owing to the winds does not seem to influence the cross-shore width of the longshore current. However, the change in the wave breaking location alters the cross-shore gradient of the radiation stresses, or the driving force of longshore currents. The implication of the model results is that an onshore wind may reduce the longshore sediment transport rate despite an increase in the distance between the breaking point and the shoreline. Conversely, an offshore wind may enhance the longshore sediment transport rate because of the stronger current (not shown here) and the increased number of plunging breakers. Notice that the wind direction is restricted to the cross-shore direction in the numerical experiment. The implication of our numerical results is not in agreement with Douglass's (1990) suggestion on the potential wind effect on the longshore sediment transport rate. Further verification of the model results against field or laboratory measurements is obviously needed.

## Summary and Conclusions

The time-domain Boussinesq wave model has been extended to including the wind effects on the nearshore wave propagation and breaking-generated currents. A new methodology for the parameterization of the wind stress has been developed based on field observations of air–sea momentum flux over shoaling waves. The drag coefficient incorporated into the Boussinesq model is not only a function of wind speed, but also depends on the wave steepness. The fairly good agreement between the drag coefficient derived from the Boussinesq model and the results predicted by the sea state dependent roughness formulas indicates that the formulation introduced to the Boussinesq model is a good representation of the wind effect on shoaling waves. Although the one-dimensional Boussiensq model incorporating the wind forcing is unable to predict the downshift of the spectral peak, the model reproduces fairly well the measured growth of the wave height on Lake George. The test confirms the effectiveness of the new wind stress parameterization in terms of the momentum or energy transfer between the wind and the water.

Wave breaking criteria have been modified to take into account the wind effect on wave breaking on the basis of the existing laboratory data. The two-dimensional version of the forced Boussinesq model with the new breaking criteria has enabled us to simulate longshore currents on a planar beach at the laboratory scale to understand the response of a current to the change in the breaking location caused by a wind. The methodology for the parameterization of the air–sea momentum flux as well as the extended Boussinesq model incorporating the wind effects appear to be a promising tool for the study of sea–swell–wind interactions, wind effects on nearshore wave propagation and horizontal circulation, and the spatial variability of the sea surface roughness length. Owing to the complex nature of the turbulent boundary layer over the ocean surface, detailed laboratory, and field experiments are required to verify the parameterization and numerical model, and to improve our understanding of air–sea processes.

## Acknowledgments

This study was supported by the Office of Naval Research through Contracts Nos. N000173-01-P-6905 and N00173-02-1-

G905. Discussions with Dr. Scott L. Douglass and assistance from Dr. Kelin Hu are sincerely acknowledged. The editor's comments are appreciated.

## References

Anctil, F., and Donelan, M. A. (1996). "Air–water momentum flux observations over shoaling waves." *J. Phys. Oceanogr.,* 26, 1344–1353.

Banner, M. L., and Peirson, W. L. (1998). "Tangential stress beneath wind driven air–water interfaces." *J. Fluid Mech.,* 364, 115–145.

Booij, N., Ris, R. C., and Holthuijsen, L. H. (1999). "A third-generation wave model for coastal regions. Part 1, Model description and validation." *J. Geophys. Res., [Oceans],* 104(C4), 7649–7666.

Bouws, E., Gunther, H., Rosenthal, W., and Vincent, C. L. (1985). "Similarity of the wind wave spectrum in finite depth water." *J. Geophys. Res., [Oceans],* 90, 975–986.

Chen, Q. (2004). "Note on the fully nonlinear Boussinesq-type equations for waves and currents over a permeable seabed." *J. Geophys. Res., [Oceans],* in press.

Chen, Q., Dalrymple, R. A., Kirby, J. T., Kennedy, A. B., and Haller, M. C. (1999). "Boussinesq modeling of a rip current system." *J. Geophys. Res., [Oceans],* 104(C9), 20,617–20,637.

Chen, Q., Kirby, J. T., Dalrymple, R. A., Kennedy, A. B., and Chawla, A. (2000). "Boussinesq modeling of wave transformation, breaking and runup. II: 2D." *J. Waterw., Port, Coastal, Ocean Eng.,* 126(1), 48–56.

Chen, Q., Kirby, J. T., Dalrymple, R. A., Shi, F., and Thornton, E. B. (2003). "Boussinesq modeling of longshore currents." *J. Geophys. Res., [Oceans],* 108 (C11), 3362–3362.

Douglass, S. L. (1990). "Influence of wind on breaking waves." *J. Waterw., Port, Coastal, Ocean Eng.,* 116(6), 651–663.

Galloway, J. S., Collins, M. B., and Moran, A. D. (1989). "Onshore/offshore wind influence on breaking waves: an empirical study." *Coastal Eng.,* 13, 305–323.

Geernaert, G. L. (1990). "Bulk parameterizations for the wind stress and heat fluxes." *Surface waves and fluxes,* Vol. 1, G. L. Geernaert and W. J. Plant, eds., Kluwer Academic, Dordrecht, The Netherlands, 91–172.

Hsu, S. A. (1988). *Coastal meteorology,* Academic, New York.

Hubertz, J. M. (1986). "Observations of local wind effects on longshore currents." *Coastal Eng.,* 10, 275–288.

Jeffereys, H. (1925). "On the formation of waves by wind. II." *Proc. R. Soc. London, Ser. A,* 110, 341–347.

Kennedy, A. B., Chen, Q., Kirby, J. T., and Dalrymple, R. A. (2000). "Boussinesq modeling of wave transformation, breaking and runup. I: 1D." *J. Waterw., Port, Coastal, Ocean Eng.,* 126(1), 39–47.

Kennedy, A. B., Kirby, J. T., and Gobbi, M. F. (2002). "Simplified higher-order Boussinesq equations I. Linear simplifications." *Coastal Eng.,* 44, 205–229.

King, D. M., and Baker, C. J. (1996). "Changes to wave parameters in the surf zone due to wind effects." *J. Hydraul. Res.,* 34 (1), 55–76.

Kirby, J. T. (2003). "Boussinesq models and applications to nearshore wave propagation, surf zone processes and wave-induced currents." *Advances in coastal modeling,* V. C. Lakhan, ed., Elsevier, New York, 1–41.

Madsen, P. A., and Schaffer, H. A. (1998). "Higher order Boussinesq-type equations: Derivation and analysis." *Philos. Trans. R. Soc. London,* 356, 3123–3184.

Madsen, P. A., and Schaffer, H. A. (1999). "A review of Boussinesq-type equations for gravity waves." *Advances in coastal and ocean engineering,* Vol. 5, P. L.-F. Liu, ed., World Scientific, Singapore, 1–94.

Schwab, D. J., Bennett, J. R., Liu, P. C., and Donelan, M. A. (1984). "Application of a simple numerical wave prediction model to Lake Erie." *J. Geophys. Res., [Oceans],* 89(C3), 3586–3592.

Shi, F., Kirby, J. T., Dalrymple, R. A., and Chen, Q. (2003). "Wave simulations in Ponce de Leon inlet using Boussinesq model." *J. Waterw., Port, Coastal, Ocean Eng.,* 129(3), 124–135.

Taylor, P. K., and Yelland, M. J. (2001). "The dependence of sea surface roughness on the height and steepness of the waves." *J. Phys. Oceanogr.,* 31, 572–590.

Visser, P. J. (1991). "Laboratory measurements of uniform longshore currents." *Coastal Eng.,* 15, 563–593.

Wei, G., Kirby, J. T., Grilli, S. T., and Subramanya, R. (1995). "A fully nonlinear Boussinesq model for surface waves. Part 1: Highly nonlinear unsteady waves." *J. Fluid Mech.,* 294, 71–92.

Wu, J. (1980). "Wind-stress coefficient over the sea surface near neutral conditions-A revisit." *J. Phys. Oceanogr.,* 10, 727–740.

Young, I. R., and Verhagen, L. A. (1996). "The growth of fetch limited waves in water of finite depth. Part 1: Total energy and peak frequency." *Coastal Eng.,* 29, 47–78.